Cooperative motion caused by thermally activated jumps in Johari-Goldstein mode

Takeaki Araki [1] and Makina Saito[2]
1) Department of Physics, Kyoto University
2) Department of Physics, Tohoku University

JST CREST Grant Number JPMJCR2095

JSPS KAKENHI 24K00592

Johari-Goldstein (JG) relaxation

・Johari–Goldstein relaxation, or slow β, is one of the secondary relaxation modes observed in glasses, supercooled liquid and other disordered materials.
・It is widely observed in polymers, small organic molecules, metallic glass, ionic glass,..
・JG relaxation is related to the mechanical properties of glasses, because the α-relaxation almost freezes and is not relevant in glasses.
・It is speculated to be a precursor of the structural α-relaxation, however the microscopic mechanism of the Johari-Goldstein relaxation has not been definitively identified.

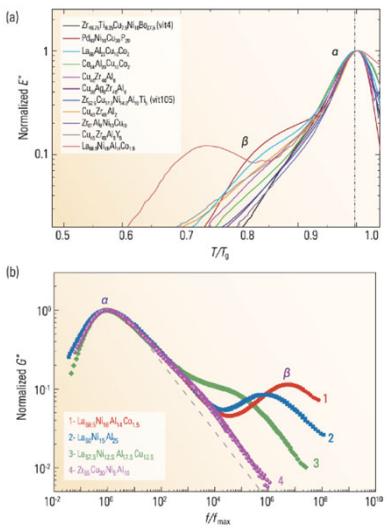

Figure 3. Comparison of the behavior of β-relaxations (measured by DMA) between typical MGs in (a) normalized temperature frame (Copyright 2011 American Physics Society) and (b) normalized frequency frame [46] (Copyright 2011 American Institute of Physics).

Y.-B. Yu, et al., Nat. Sci. Rev. 1, 429 (2014)

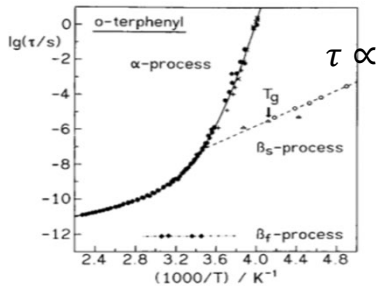

$\tau \propto \exp(E/k_{\mathrm{B}}T)$

Figure 3. Compilation of various relaxation times measured for *o*-terphenyl. α-relaxation: dielectric relaxation (+); dynamic Kerr effect (×); light scattering (⊕); NMR (●). β_s-relaxation: dielectric relaxation (○); time-resolved optical spectroscopy (△). β_f-relaxation: neutron scattering (◆). The ordinate is the base 10 logarithm. Solid and dashed lines are guides for the eye. Different experimental techniques often give similar relaxation times in one-component supercooled liquids. Data sources are given in ref 10. Reproduced with permission from ref 9. Copyright 1994 North-Holland.

M. D. Ediger, et al. J. Chem. Phys. 100, 13200 (1996)

K. L. Ngai, Relaxation and diffusion in complex systems. (Springer, Berlin, 2011).

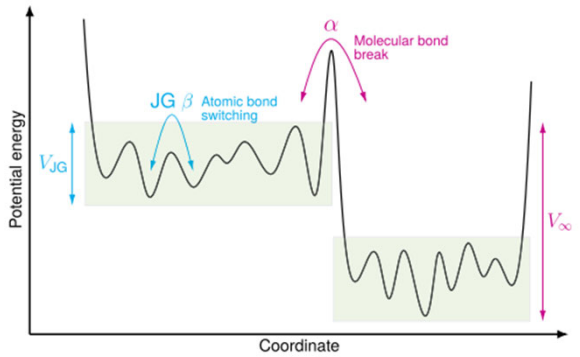

Fig. 1. Schematic summary of this paper. A newly introduced quantity, which is a variance of time series of the inherent structure potential energy, shows the hierarchical structure of topography. From a real-space perspective, the switching of atomic bonds corresponds to JG β relaxation. Correlation between low-frequency vibrational modes and the subsequent relaxation persists for the α relaxation time.

K. Shiraishi et al., PNAS 120, e2215153120 (2023)

Purpose of this work

The purpose of this work is to clarify the physical mechanisms of Johari-Goldstein mode, by means of microscopic experiments and molecular dynamics simulations.

Johari's scenario
The thermally activated motion occurs in restricted regions called "islands of mobility"

Williams and Watts scenario
All molecules partially relax due to the thermal activated motion

Or others?

We use an ionic glass $Ca_{0.4}K_{0.6}(NO_3)_{1.4}$ and metallic glass ZrCuAl as model systems.
They are accessible with our experimental and numerical methods.

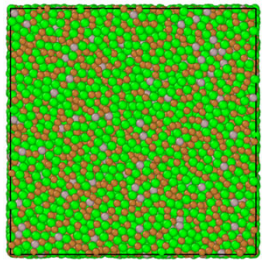

ZrCuAl

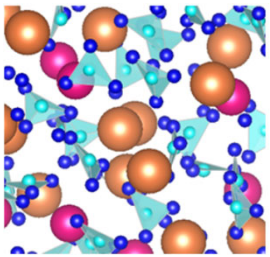

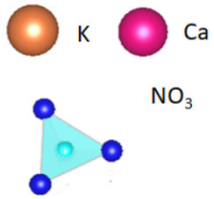

$CaKNO_3$

Quasi-elastic scattering using gamma-rays

It can measure slow dynamics ranging 10-1000nsec in atomistic length scale.

Applicable to microscopic slow dynamics in liquids and soft matters

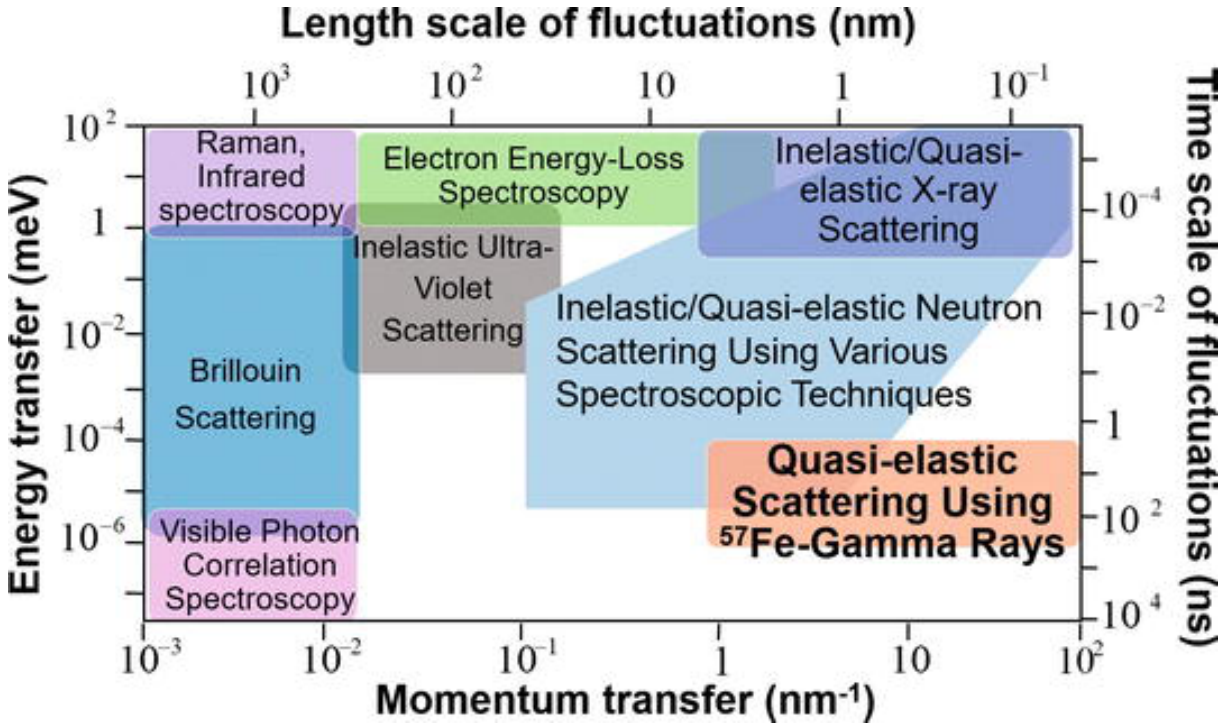

JG relaxation in glycerol

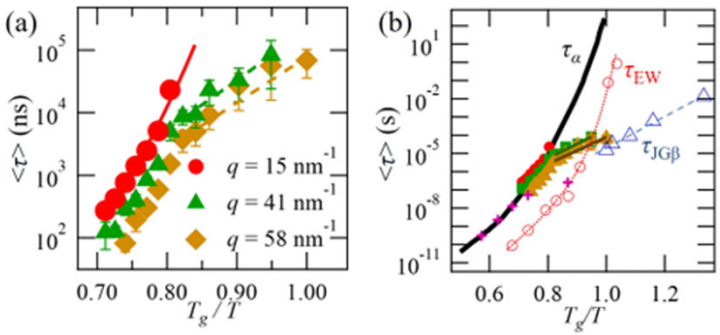

M. Saito, et al., Sci. Rep. 7, 12558 (2017).
M. Saito, et al., Phys. Rev. Lett. 109, 115705 (2012).
T. Kanaya, et al., J. Chem. Phys. 140, 144906 (2014).
M. Saito, et al., Phys. Rev. E 105, L012605 (2022).

Ionic glass $Ca_{0.4}K_{0.6}(NO_3)_{1.4}$

$T_g = 336K$

Mechanical response

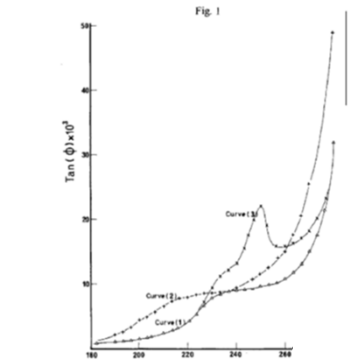

A plot of tan ϕ against temperature at (curve (1)) 1 Hz and (curve (2)) 45 mol% $Ca(NO_3)_2$·55 mol% KNO_3 glass during cooling of measurements at 1 Hz made during the heating of the same sa this plot is caused by ice formed on the surface of the sam

C. Mai, et al., *Philos. Mag. B* **50**, 657 (1985).

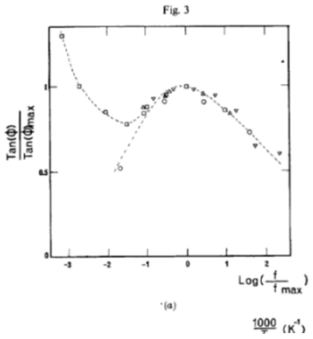

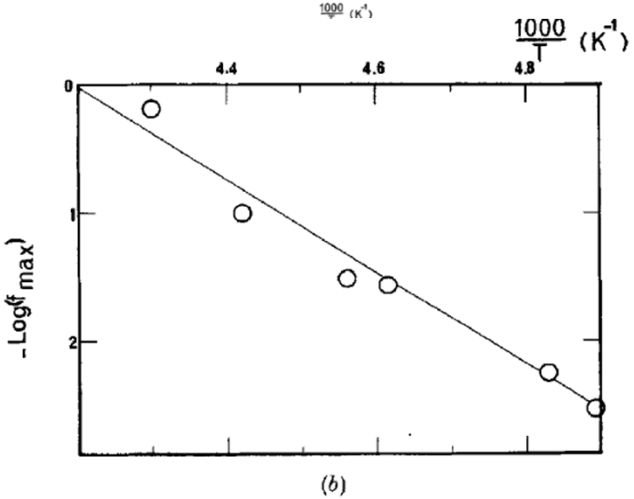

(*a*) Normalized plots of tan ϕ against frequency below T_g. (▽) 203 K; (○) 219 K; (△) 226 K; (□) 232 K. (*b*) Arrhenius plot of the frequency of the maximum in tan ϕ of the nitrate glass.

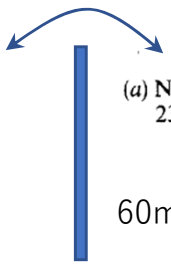

60mm

1mm

0.1~1Hz

Dielectric spectroscopy

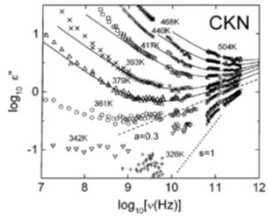

FIG. 1. Frequency dependence of the dielectric loss of CKN for various temperatures (double-logarithmic plot). The solid lines represent fits using Eq. (1) with $a = 0.3$ and $b = 0.54$.

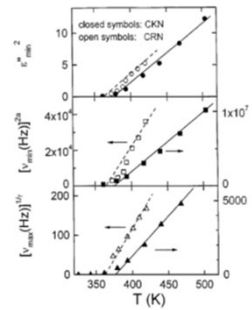

4. Temperature dependence of height and position of the tric loss minimum and of the α-peak position of CKN d symbols) and CRN (open symbols). Representations been chosen that result in straight lines according to the ctions of the MCT. The solid lines are consistent with a l temperature of $T_c = 375$ K for CKN, the dashed lines $T_c = 365$ K for CRN.

P. Lunkenheimer, et al., Phys. Rev. Lett. 78, 2995 (1997)

Neutron spin echo

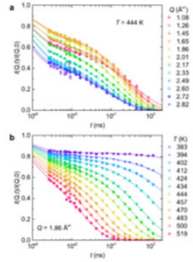

Fig. 2 Representative intermediate scattering functions of CKN. **a** T = 444 K at various Q's between 1.08 Å⁻¹ and 2.82 Å⁻¹. **b** Q = 1.86 Å⁻¹ at various temperatures between 383 K and 519 K. The solid lines represent fit to Eq. (1). Error bars represent one standard error and are smaller than the symbol size. Source data are provided as a Source Data file.

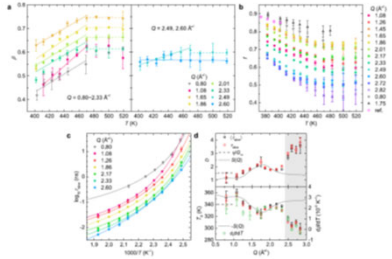

Fig. 4 Temperature behavior of the relaxation dynamics at different length scales. a Exponent β as a function of temperature (left panel: Q = 0.80 Å⁻¹ 2.33 Å⁻¹, right panel: Q = 2.49 Å⁻¹ and 2.60 Å⁻¹, solid lines are representative linear fit and dash lines are guide for the eye). **b** Temperature dependenc of effective Debye–Waller factor f at various Q's. The open diamonds are adapted from Ref. [30] at Q = 1.86 Å⁻¹. **c** Logarithmic relaxation time $\tau_{\alpha,\mu m}$ as a function of 1000/T with VFT fits (Eq. (2)). To make it easier for the reader to discern the curves, the data for only representative Q's are shower in **a** and **c**, the rest of the data can be found in Supplementary Figs. 5 and 6. The half-filled triangles in **a**–**c** represent the results measured on NGA-NSI **d** Q-dependence of D (upper panel) and T_0 (lower panel) obtained from the VFT fit to $\tau_{\alpha,\mu m}$ (red circles), $(\tau_{\alpha,\mu m})$ (black squares), and the macroscopic shear relaxation time $(\tau) = \eta/G_\infty$ (dash lines) [see Supplementary Figs. 7a and 9 for the VFT fit to (τ) and $(\tau_{\alpha,\mu m})$]. diamonds in the lower panel are Q-dependence of $d\beta/dT$ (right axis). The solid line in the upper panel of **d** is the static structure factor S(Q) measured at T = 480 K, and that in the lowe panel is ~S(Q). Error bars represent one standard error and where not seen they are smaller than the symbol size. Source data are provided as a Sourc Data file.

P. Luo, Nat. Comm. 13, 2092 (2022)

Ionic glass $Ca_{0.4}K_{0.6}(NO_3)_{1.4}$: Gamma ray QES

Relaxation time vs T

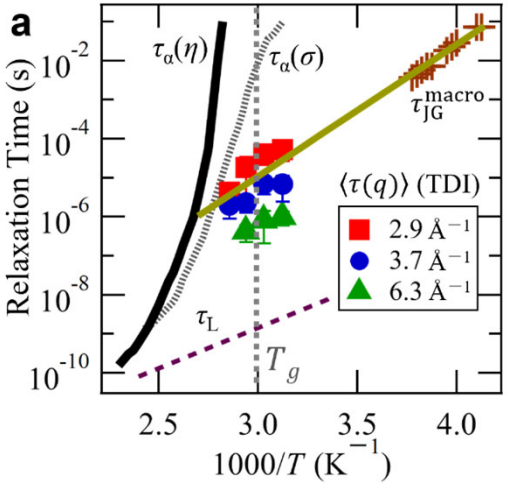

Relaxation time vs q

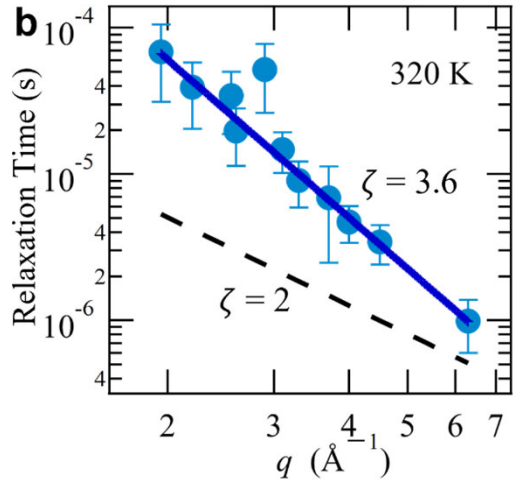

C. Mai, et al., *Philos. Mag. B* **50**, 657 (1985).

Stretching parameter of Intermediate scattering function

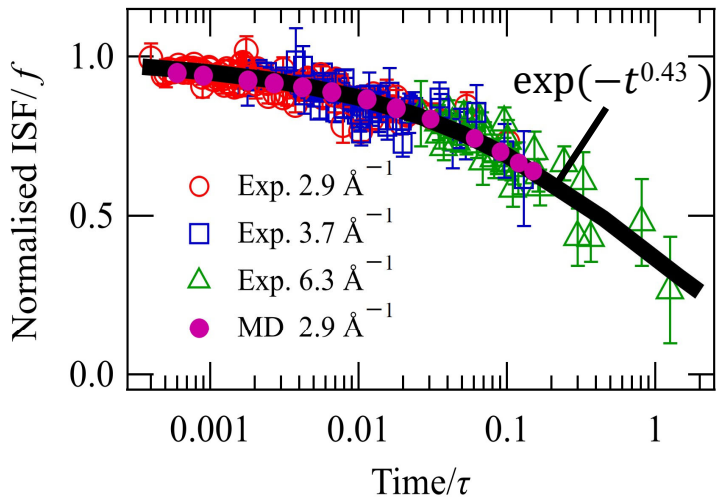

Structure factor

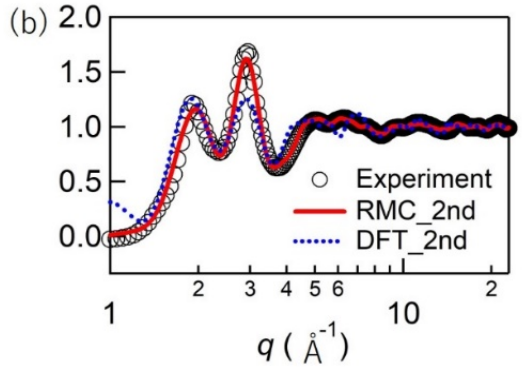

M. Saito, T. Araki, Y. Onodera, K. Ohara, M. Seto, Y. Yoda, Y. Wakabayashi, submitted.

Kohlausch-Williams-Watts(KWW)

$$F(q,t) = A\exp[-(t/\tau_\beta)^{\beta_{\mathrm{KWW}}}]$$

(1) Intermediate scattering at $q = 2.9\text{Å}^{-1}$ corresponds to mechanical relaxation
(2) Wave number dependence of the relaxation time $\tau \propto q^{-\zeta}$ ($\zeta \sim 3.6$)
(3) Anomalous stretched exponential parameter $\beta_{\mathrm{KWW}} \sim 0.43$

All-atom molecular dynamics simulation

Born-Mayer-Huggins potential

$$U_{\alpha\beta}(r) = A_{\alpha\beta}\exp\left(-\frac{r}{\sigma_{\alpha\beta}}\right) - \frac{C_{\alpha\beta}}{r^2} + \frac{q_\alpha q_\beta}{r}$$

$$U_{\mathrm{NO\ bond}}(r) = K_{\mathrm{bond}}(r - r_0)^2$$

$$U_{\mathrm{ONO\ angle}}(\theta) = K_{\mathrm{angle}}(\theta - \theta_0)^2$$

$NO_3^{-1}(504)$ $K^+(216)$ $Ca^{2+}(144)$

$$A_{\mathrm{N-N}} = 33.7\mathrm{Mcal/mol}, \sigma_{\mathrm{N-N}} = 0.2646\text{Å}, C_{\mathrm{N-N}} = 259.3\mathrm{kcal}/(\mathrm{mol}\cdot\text{Å}^6)$$

$$A_{\mathrm{O-O}} = 62.2\mathrm{Mcal/mol}, \sigma_{\mathrm{O-O}} = 0.23926\text{Å}, C_{\mathrm{O-O}} = 259.3\mathrm{kcal}/(\mathrm{mol}\cdot\text{Å}^6)$$

$$A_{\mathrm{K-K}} = 36.1\mathrm{Mcal/mol}, \sigma_{\mathrm{K-K}} = 0.3370\text{Å}, C_{\mathrm{K-K}} = 350.2\mathrm{kcal}/(\mathrm{mol}\cdot\text{Å}^6)$$

$$A_{\mathrm{Ca-}Ca} = 36.1\mathrm{Mcal/mol}, \sigma_{\mathrm{Ca-Ca}} = 0.3278\text{Å}, C_{\mathrm{Ca-Ca}} = 350.2\mathrm{kcal}/(\mathrm{mol}\cdot\text{Å}^6)$$

$$K_{\mathrm{bond}} = 761.2\ \mathrm{kcal}/(\mathrm{mol}\cdot\text{Å}^2), r_0 = 1.219(\text{Å})$$

$$K_{\mathrm{angle}} = 77.15/\mathrm{mol}, \theta_0 = 125.13°$$

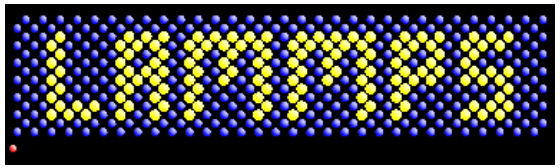

Cooling rate: $-1\mathrm{K/nsec}$ (NPT)
Equilibration time : $1\mu\mathrm{sec}$ (NPT)
Production run: $12\mu\mathrm{sec}$ (NVT)
10 sampling simulations.

Samples with the two longest and shorted relaxation times are removed from the averaging.

F. Signorini, J.-L. Barrat and M. L. Klein, J. Chem. Phys. 92, 1294 (1990)

Static properties of Ionic glass $Ca_{0.4}K_{0.6}(NO_3)_{1.4}$

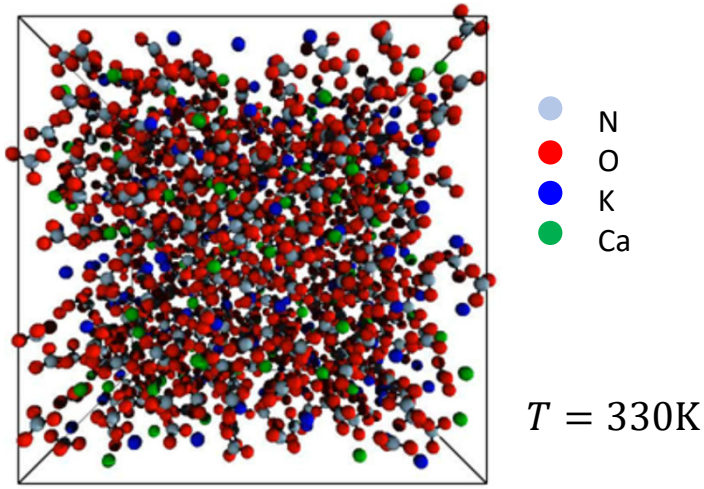

Density vs T

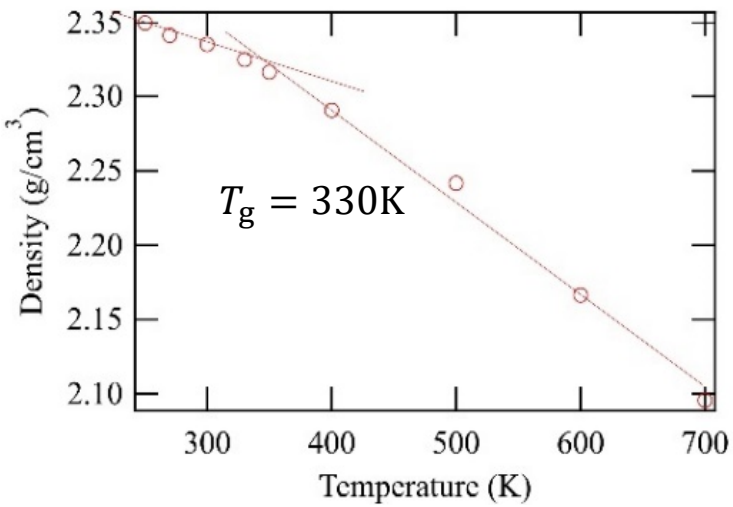

Radial distribution function

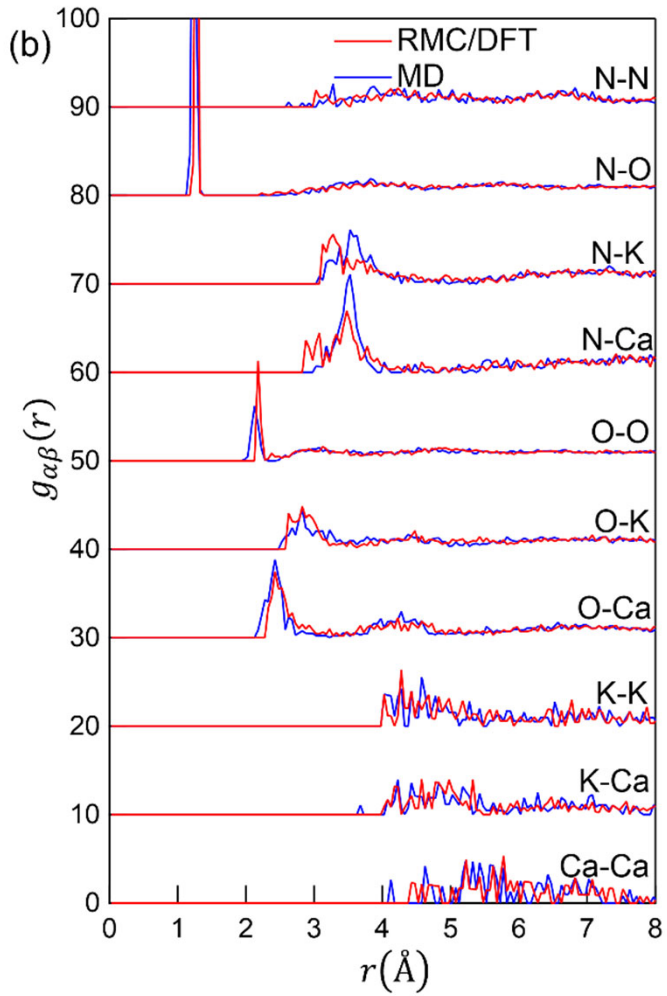

RMC/DFT performed by Yohei Onodera, Koji Ohara

Dynamic properties of $Ca_{0.4}K_{0.6}(NO_3)_{1.4}$

Mean square displacement

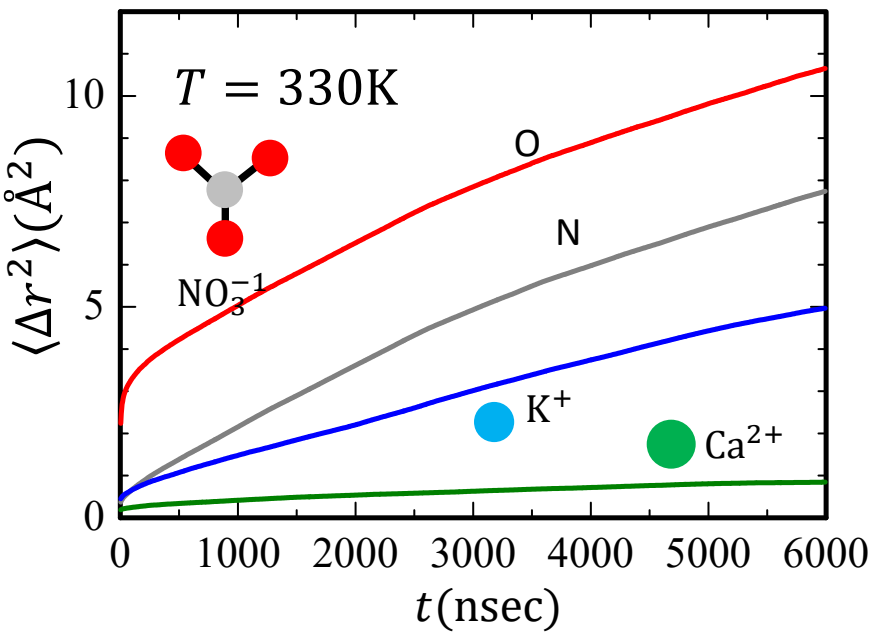

Intermediate scattering function

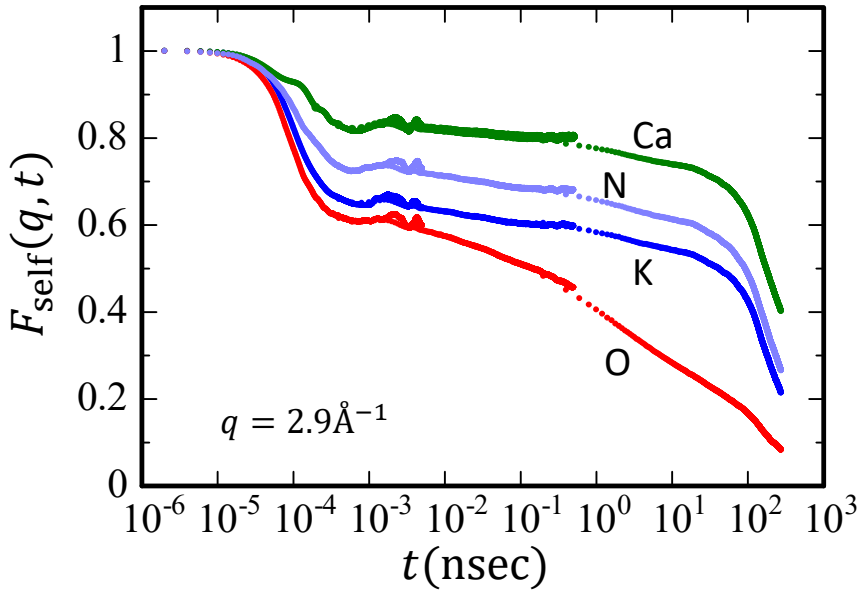

$$F_{self}(q,t) = \frac{1}{N}\sum_j \left\langle \exp\{i\boldsymbol{q}\cdot\left(\boldsymbol{r}_j(t) - \boldsymbol{r}_j(0)\right)\}\right\rangle$$

Rotational motion

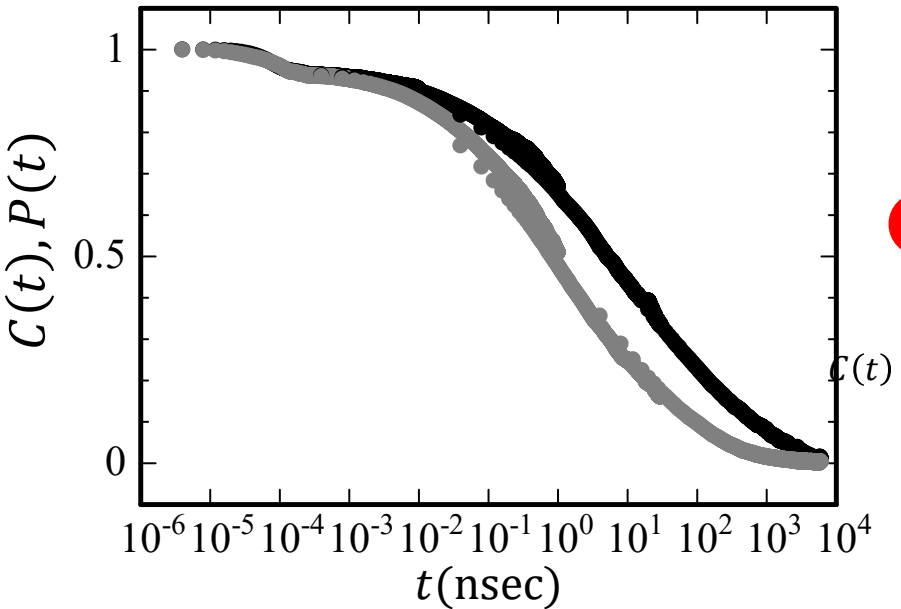

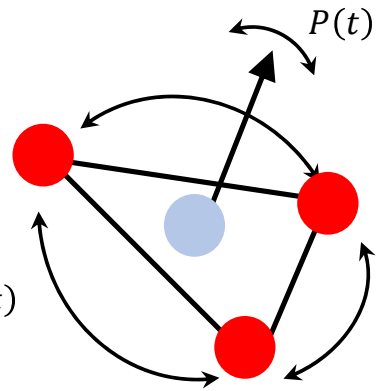

Near T_g, the rotational motion of NO_3 (or the motion of the oxygen) is much faster than the translational motions of ions.
We focus on the translational motions.

Dynamic properties of $Ca_{0.4}K_{0.6}(NO_3)_{1.4}$

Total Intermediate scattering function

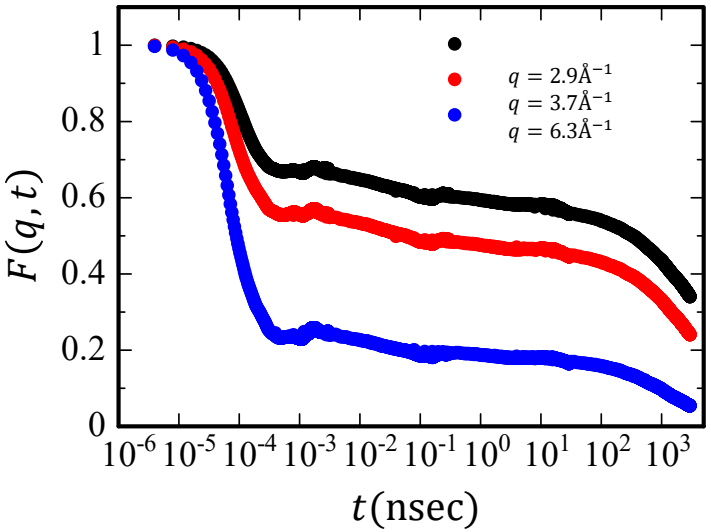

Stretching parameter vs q

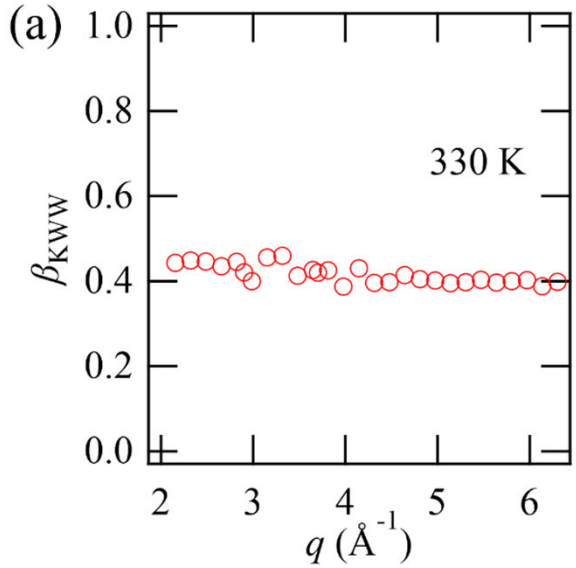

Relaxation time vs q

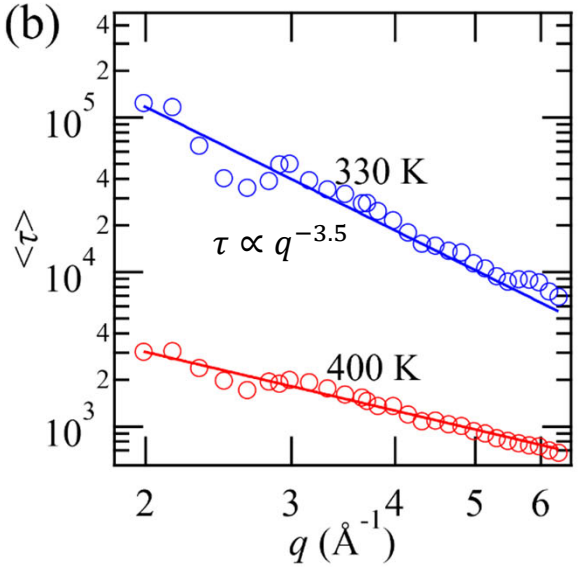

$$F(q,t) = \frac{1}{N_p S(q)} \left\langle \sum_{i,j} m_i m_j \frac{4\pi \sin q|\boldsymbol{r}_i(t) - \boldsymbol{r}_j(0)|}{q|\boldsymbol{r}_i(t) - \boldsymbol{r}_j(0)|} \right\rangle$$

$$F(q,t) = A \exp[-(t/\tau_\beta)^{\beta_{KWW}}]$$

(1) Intermediate scattering at $q = 2.9Å^{-1}$ corresponds to mechanical relaxation
(2) Wave number dependence of the relaxation time $\tau \propto q^{-\zeta}$ ($\zeta \sim 3.6$)
(3) Anomalous stretched exponential parameter $\beta_{KWW} \sim 0.43$

Mechanical relaxation

Intermediate scattering function and mechanical response

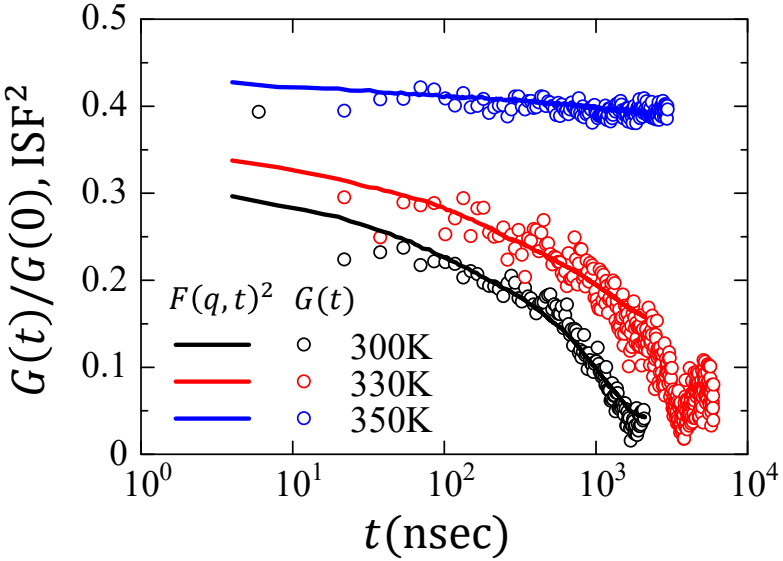

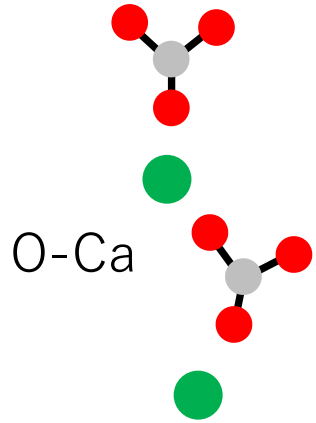

Relaxation time vs T

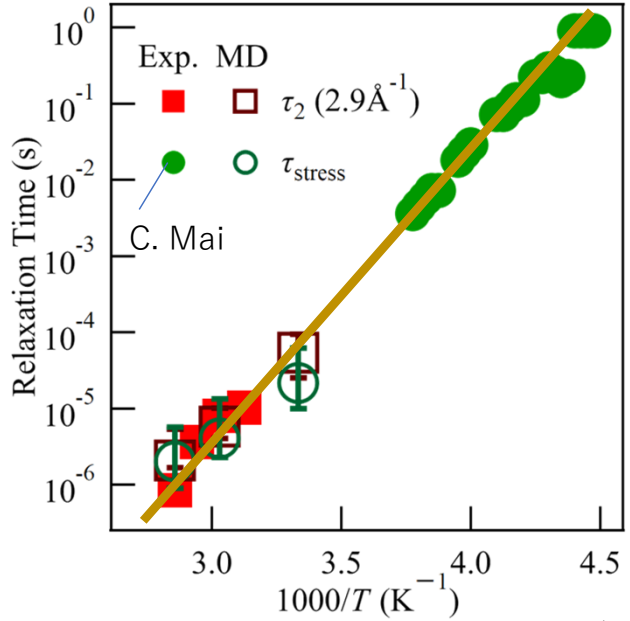

C. Mai, et al., *Philos. Mag. B* **50**, 657 (1985).

$$G(t) = \frac{V}{kT}\langle \Pi_{xy}(t)\Pi_{xy}(t)\rangle$$

$$\Pi_{xy} = \frac{1}{V}\sum_i \left[-mv_{i,x}(t)v_{i,y}(t) + \frac{1}{2}\sum_j f_{ij,x}(t)(r_{i,y}(t) - r_{j,y}(t))\right]$$

Mode coupling approximation

$$G(t) = \frac{k_B T}{60\pi^2}\int dq q^4 \mathrm{Tr}\left[\left\{\frac{dc(q)}{dq}\cdot F(q,t)\right\}^2\right]$$

(1) Intermediate scattering at $q = 2.9\text{Å}^{-1}$ corresponds to mechanical relaxation (the correlation between O and Ca)
(2) Wave number dependence of the relaxation time $\tau \propto q^{-\zeta}$ ($\zeta \sim 3.6$)
(3) Anomalous stretched exponential parameter $\beta_{\mathrm{KWW}} \sim 0.43$

We can visualize the real-space relaxation picture of the JG mode by analyzing molecular dynamics simulation, which are validated by QEGS experiments.

Trajectories of ions

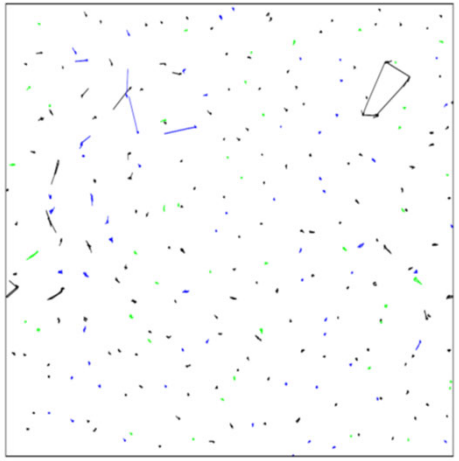

$\Delta t = 60\text{nsec}$

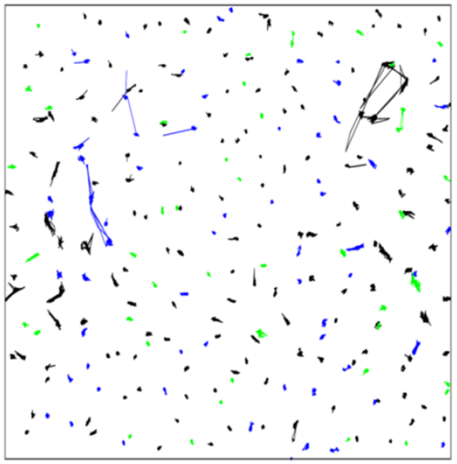

$\Delta t = 600\text{nsec}$

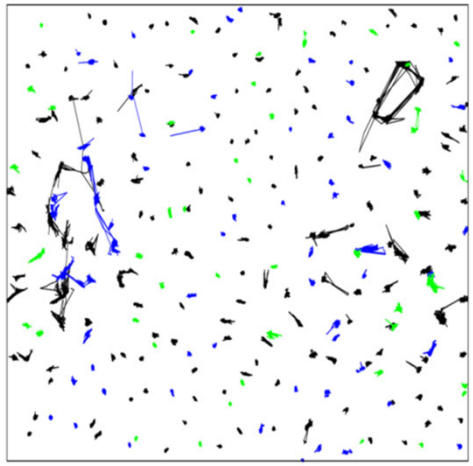

$\Delta t = 1200\text{nsec}$

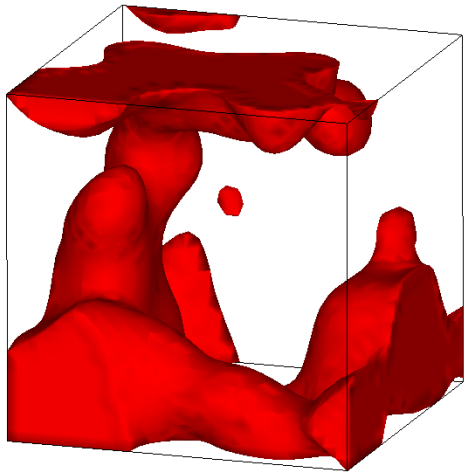

N
K
Ca

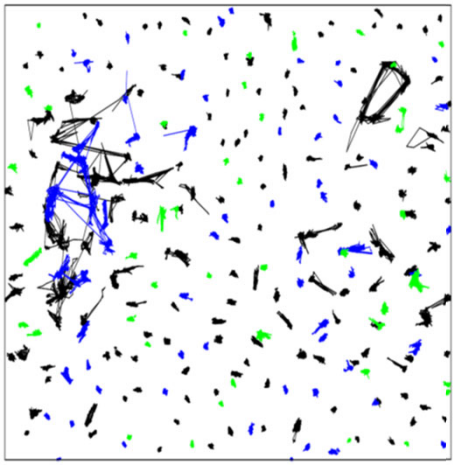

$\Delta t = 3000\text{nsec}$

$31.9\text{Å}, \Delta z = 10\text{Å}$

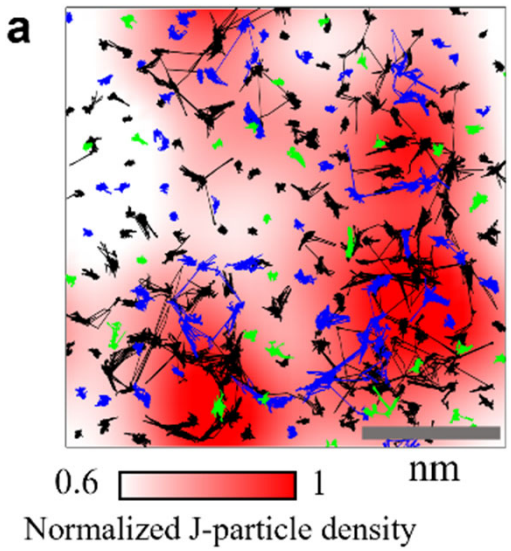

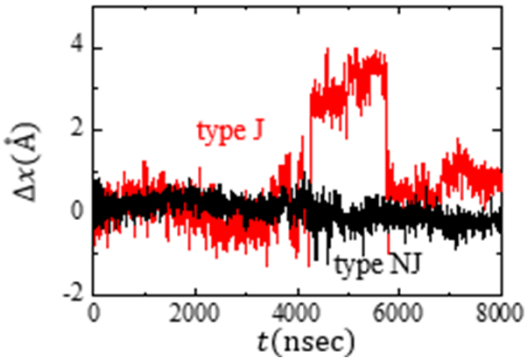

We defined a movement larger than 2.5 Å in 4 nsec as a jump motion.

We call the particles exhibiting no jump in 12 μsec **type NJ** (non-jump) and the others **type J** (jump).

Correlation between jumping and non-jumping particles

Mean square displacement

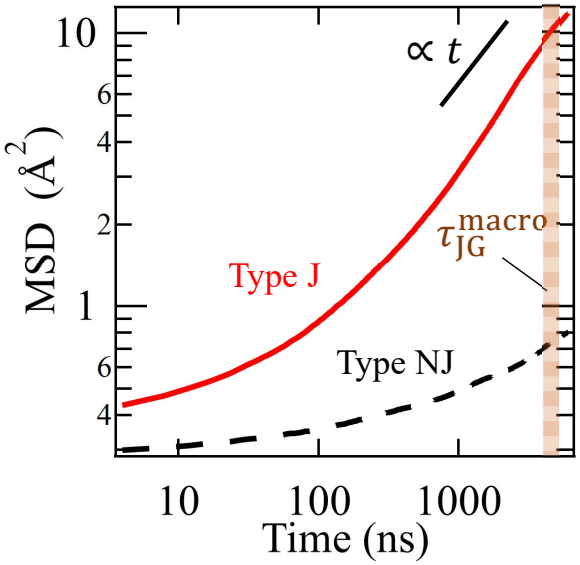

van Hove function

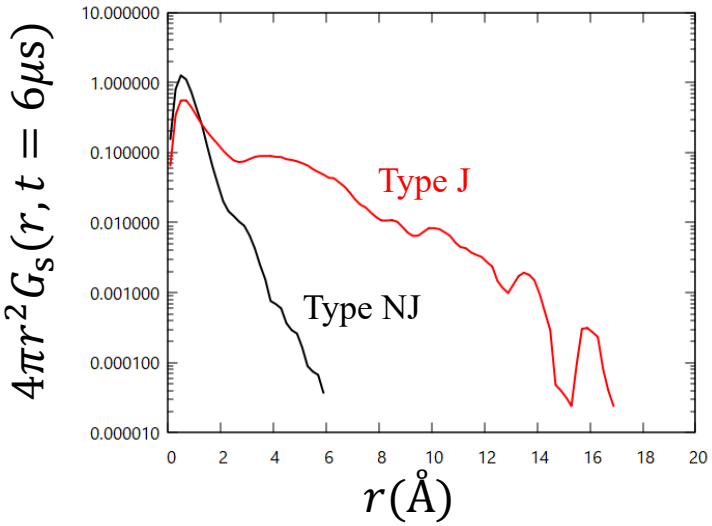

Auto-correlation of virial stress

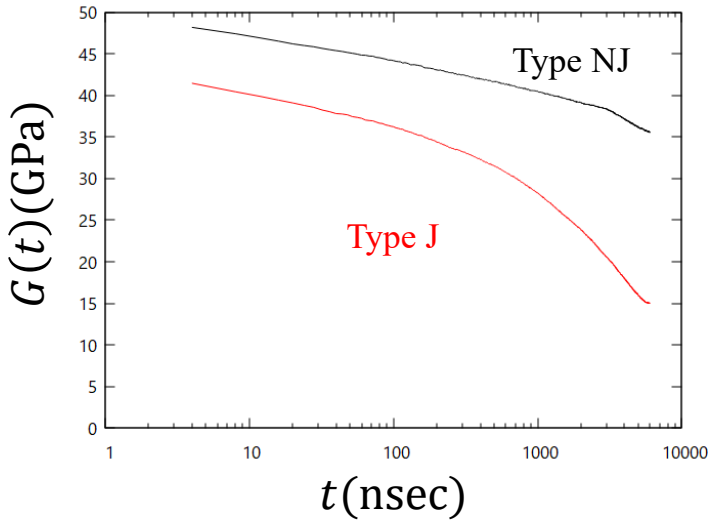

Radial distribution function

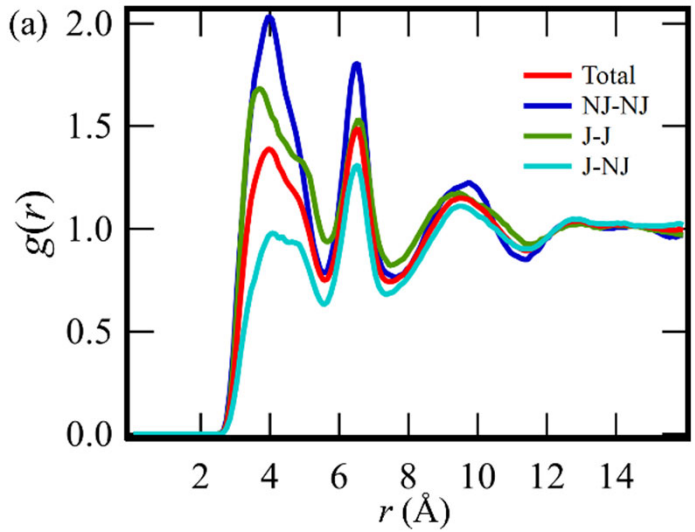

Type NJ particles exhibit small, but non-negligible sub-angstrom scale motion in the JG time scale even without the jump motions.

Type J particles are loosely packed compared to type NJ ones.

Correlation between jumping and non-jumping particles

Auto-correlation of virial stress

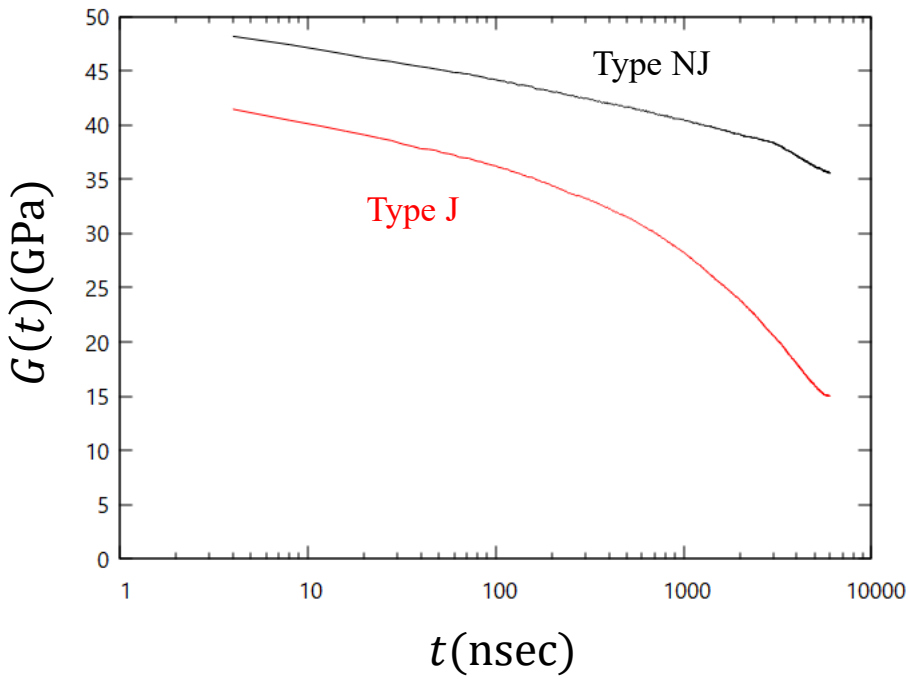

Stress relaxation for type NJ near type J after their jumps

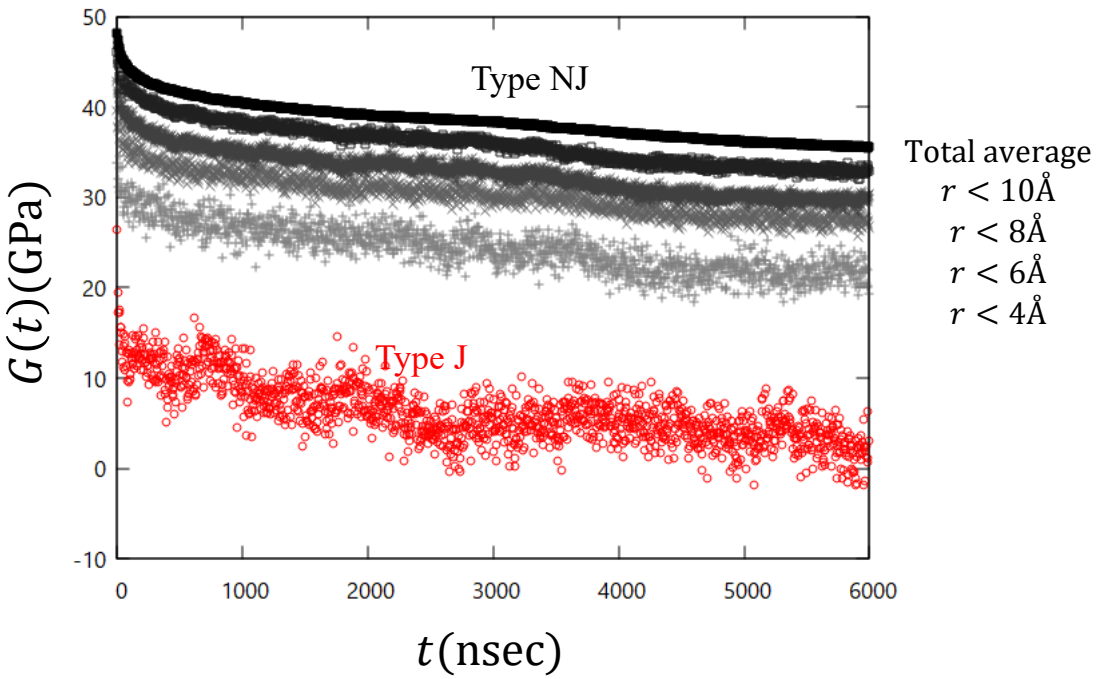

$$\sigma_{ixy}(t) = -mv_{i,x}(t)v_{i,y}(t) + \frac{1}{2}\sum_j f_{ij,x}(t)(r_{i,y}(t) - r_{j,y}(t))$$

$$G(t) = \frac{v_0}{N_X kT}\sum_{i\in\text{type X}} \langle \sigma_{ixy}(t+t_J)\sigma_{ixy}(t_J)\rangle$$

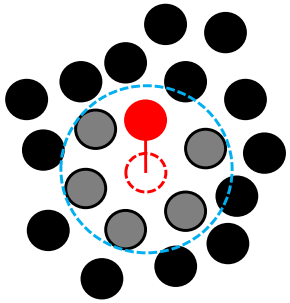

The motions of type NJ particles are very small (~ 0.1Å), their stress relaxation is not negligible.
The stress relaxation of type NJ is triggered by the thermally activated motion of type J.

Correlated motion caused by thermal jumps

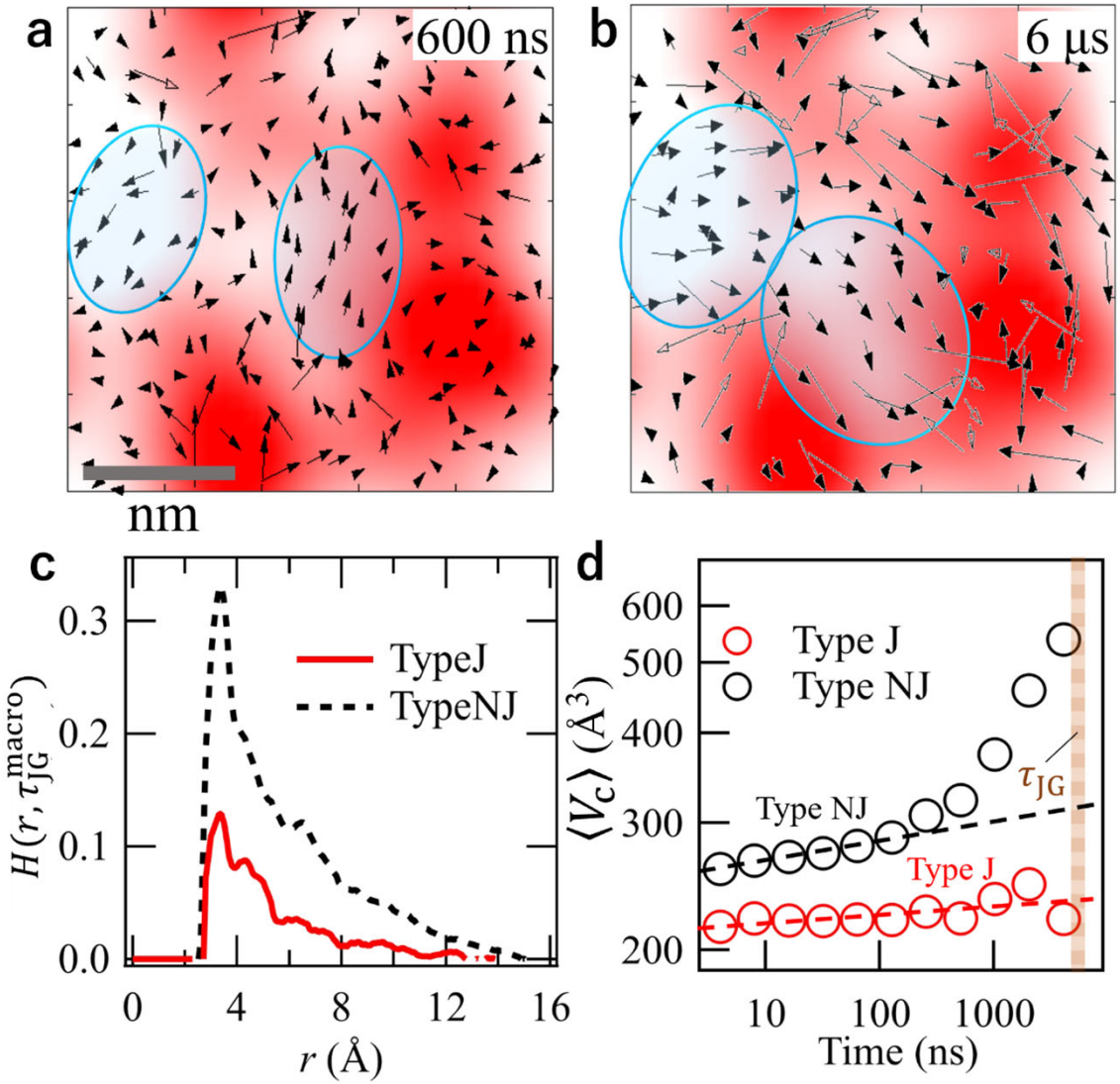

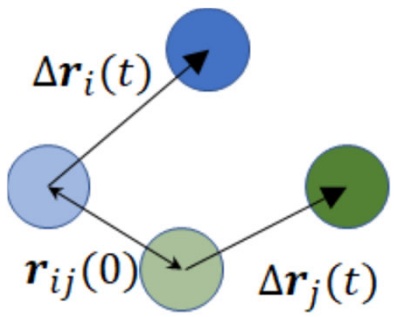

Correlation function

$$H(r,t) = \frac{V}{4\pi r^2 N_p^2 g(r)} \times \sum_{i \neq j} \langle \Delta \hat{\boldsymbol{r}}_i(t) \cdot \Delta \hat{\boldsymbol{r}}_j(t) \delta(r - |\boldsymbol{r}_i(0) - \boldsymbol{r}_j(0)|) \rangle$$

Cluster size

$$V_c(t) = 4\pi \int \mathrm{d}r r^2 H(r,t)$$

The correlation of the directions of the motion for type NJ is more remarkable than that for type, although the motions are very slow.

q −dependence of the relaxation time for individual ions

ISF for individual particles

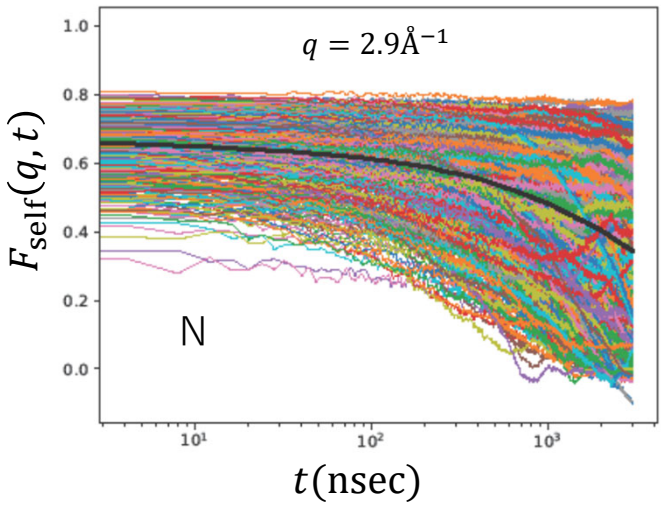

$$F(q,t) = A\exp[-(t/\tau_\beta)^\beta]$$

Relaxation time vs wave number

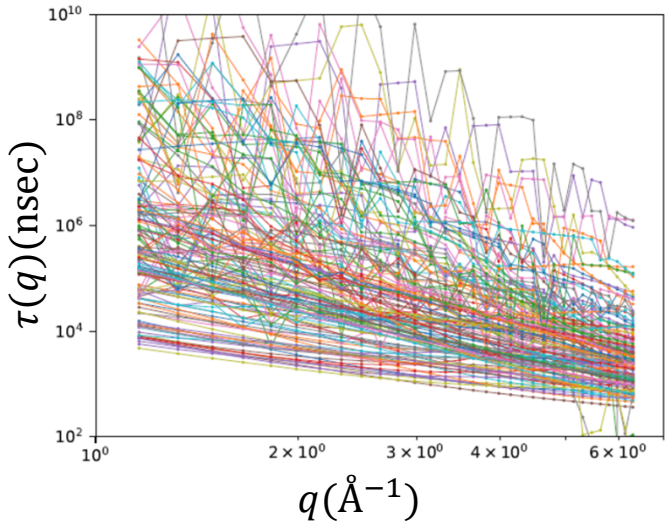

$$\tau = \tau_0(q/q_0)^{-\zeta}$$

Histogram of the power low index ζ

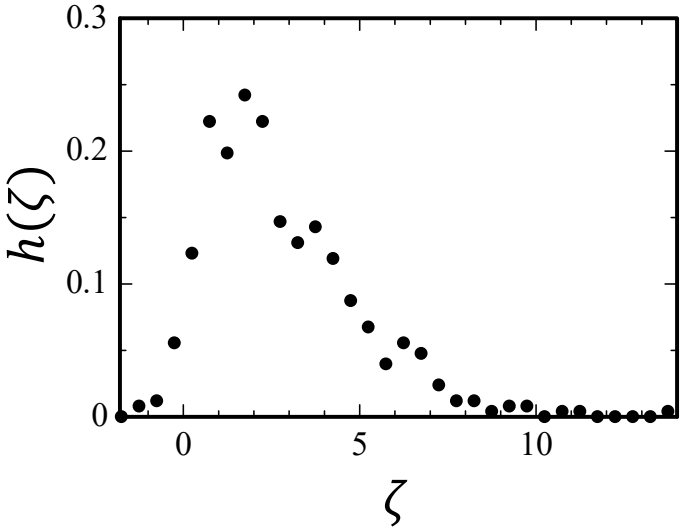

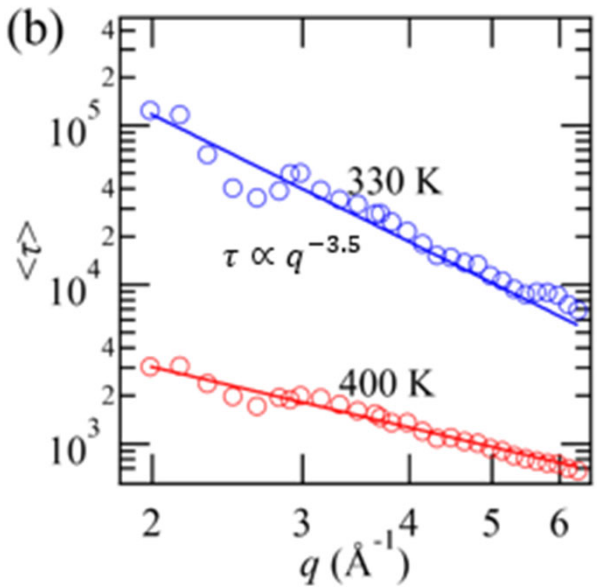

Correlation motions of directions of particle motions

Correlation motions of directions of particle motions

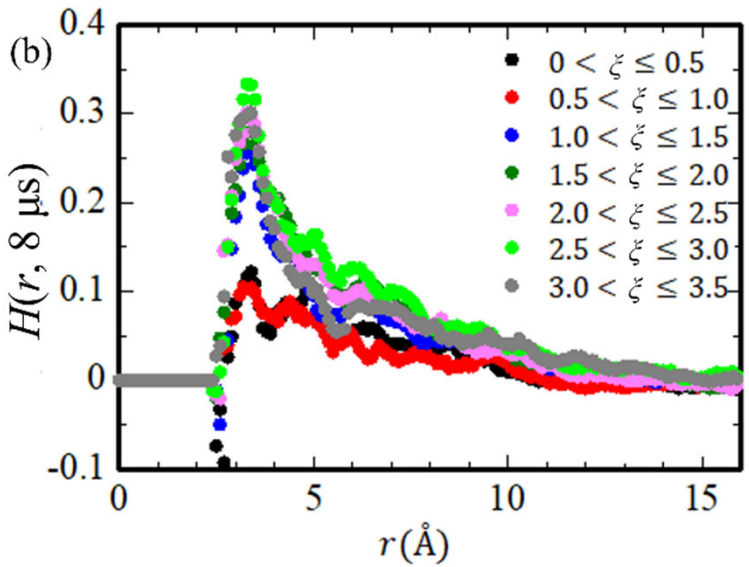

Cluster size vs ζ

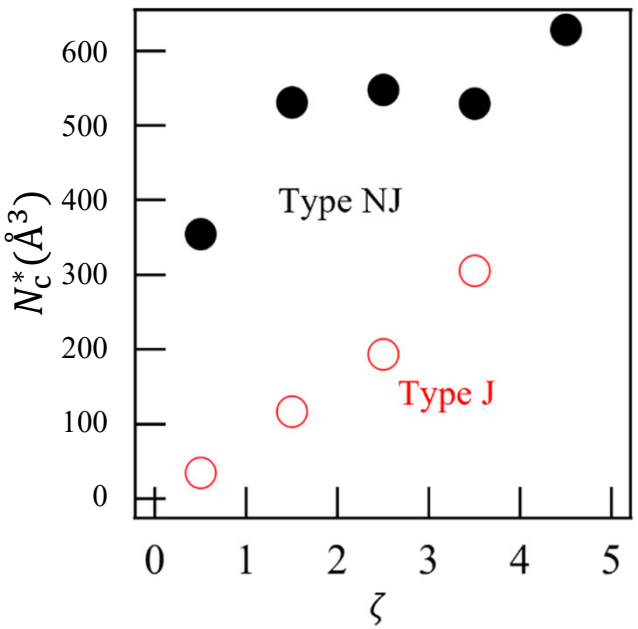

$$N_c(t) = \int dr\, 4\pi r^2 H(r,t)$$

The particles having the larger power tend to belong to larger clusters.
The large q-dependence comes from the confinement effect due to lower mobility of larger clusters.

q-dependence of the relaxation time

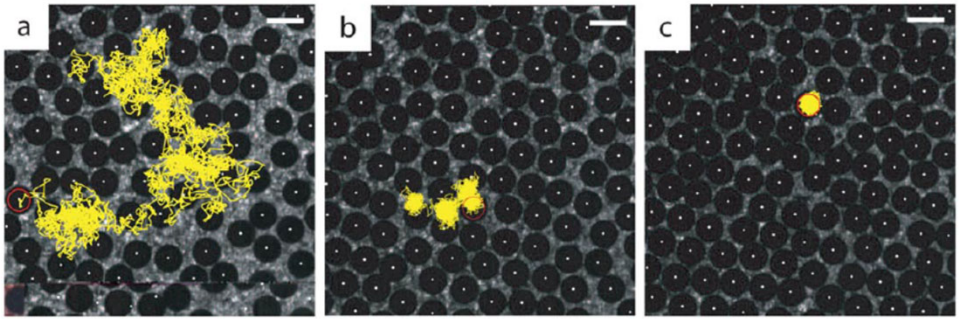

FIG. 1 (color online). Experimental frames with superposed typical trajectories of a single particle: (a) $\phi = 0.567$, (b) $\phi = 0.701$, and (c) $\phi = 0.749$. Note that even though only a single trajectory is shown for each ϕ, particle tracking and statistics were performed over all particles within the imaging window. The scale bar is 2 mm.

P. M. Reis, Phys. Rev. Lett. 98, 188301 (2007)

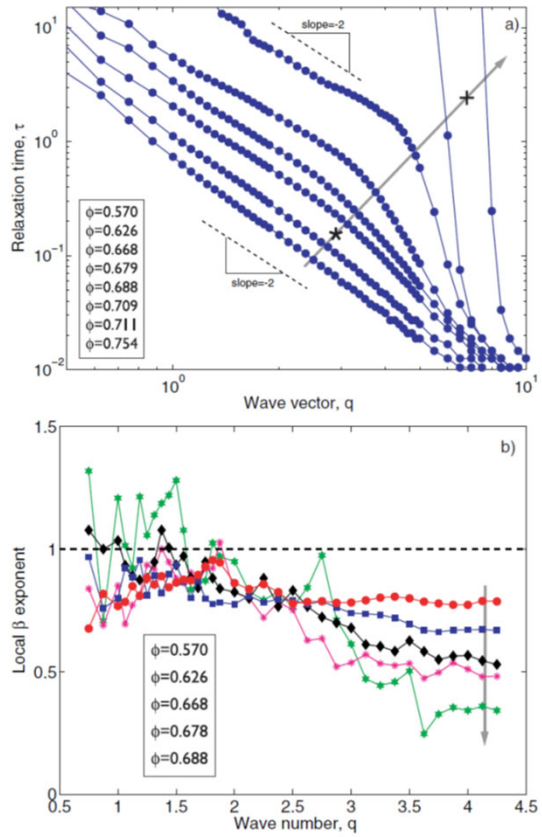

FIG. 4 (color online). (a) Wave vector dependence of the relaxation time, τ, and (b) local stretching exponent, β, for various values of filling fraction. The arrows point in the direction of increasing ϕ, and the numerical values of ϕ are given in the boxes. Along the arrow, the symbols ($*$) and ($+$) are located at ϕ_l and ϕ_s, respectively.

For large q, the Brownian scaling breaks down to a stretched exponential with $\beta < 1$, which can be attributed to the presence of dynamic heterogeneities due to caging.

Johari-Goldstein mode in CKN

The QEGS for CKN experiments revealed
(1) Intermediate scattering function at $q = 2.9\text{Å}^{-1}$ corresponds to the mechanical response.
(2) The wave number dependence of the relaxation time obeys $q^{-3.6}$.
(3) Anomalous stretched parameter 0.43.

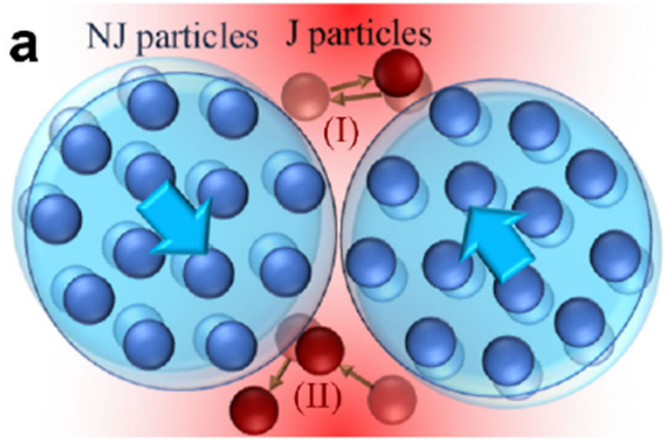

The molecular dynamics simulation reproduced them quantitively.
The detailed analyses of the simulation which are validated by the experiment can visualize the microscopic origin of the JG mode.

We found that the unexpected collective motion of non-jumping particles in the JG time scale.
The anomalous q-dependence of the JG relaxation time is due to the collective motion of the NJ particles.
The thermally activated jumps cause the small motions and the stress relaxation around them.

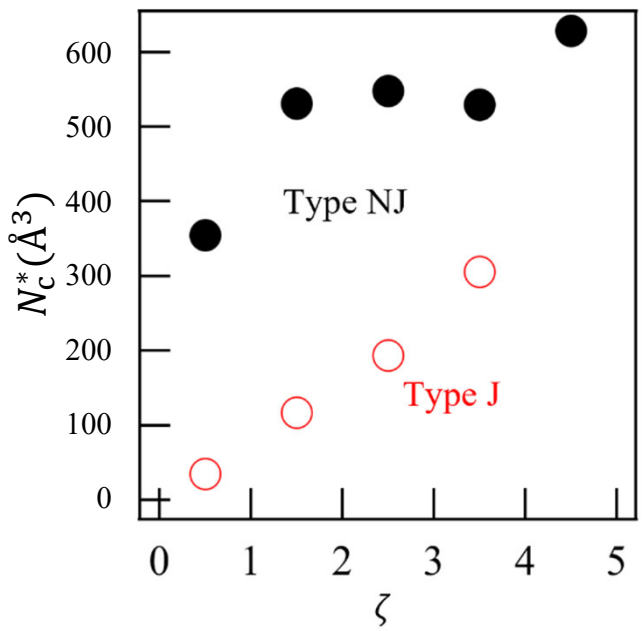

$\tau \propto q^{-\zeta}$

Johari-Goldstein relaxation in metallic glasses

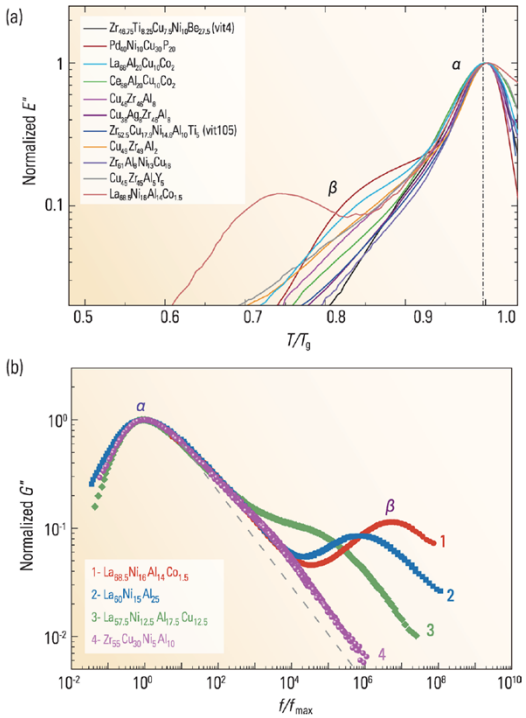

Figure 3. Comparison of the behavior of β-relaxations (measured by DMA) between typical MGs in (a) normalized temperature frame (Copyright 2011 American Physics Society) and (b) normalized frequency frame [46] (Copyright 2011 American Institute of Physics).

Y.-B. Yu, et al., Nat. Sci. Rev. 1, 429 (2014)

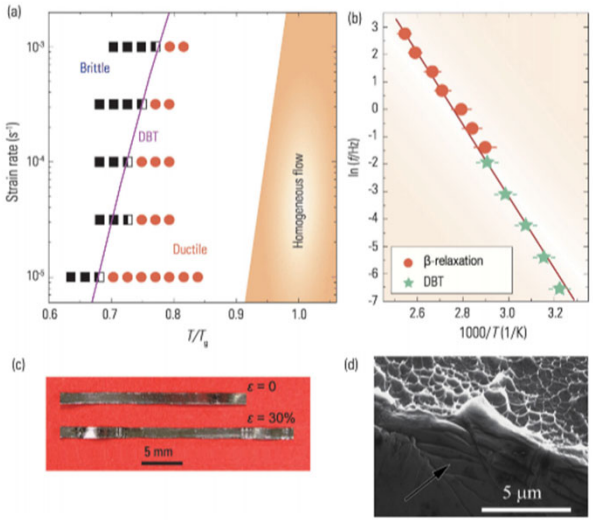

Figure 17. (a) Deformation mode map summarizing tensile tests at different temperatures and strain rates, see [35] for the meanings of the symbols. (b) Arrhenius plot of DBT and β-relaxation of the MG. (c) Image of the MG before and after tensile testing. (d) SEM image of a La MG ductile fracture surface (Copyright 2012 American Physics Society).

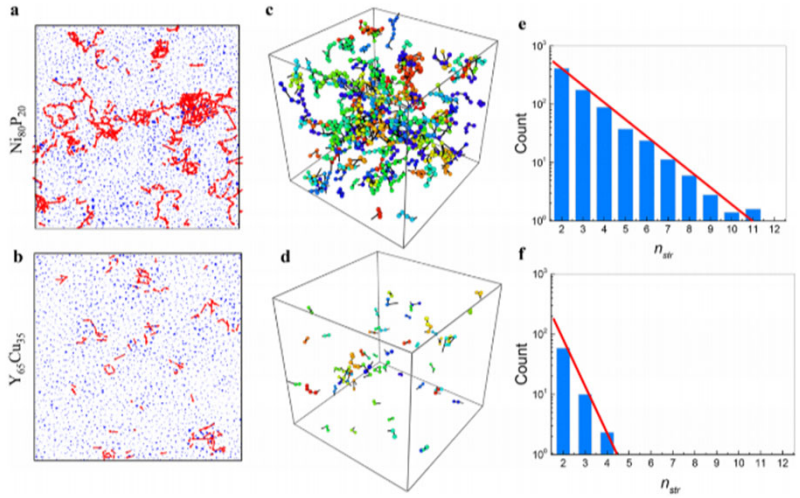

Figure 3. String-like cooperative atomic jumps in MGs. Atomic displacement vectors for (a) $Ni_{80}P_{20}$ and (b) $Y_{65}Cu_{35}$ MGs; the slice is 1 nm. String-like atomic displacements for (c) $Ni_{80}P_{20}$ and (d) $Y_{65}Cu_{35}$ MGs. Statistics of the number of atoms in string-like motions (N_{str}) for (e) $Ni_{80}P_{20}$ and (f) $Y_{65}Cu_{35}$ MGs. The red smooth curves in (e) and (f) are fitted by an exponential decay function.

Y.-B. Yu, et al., Phys. Chem. Lett. 9, 5877 (2018)

Some metallic glasses exhibit large secondary relaxation, which is considered to be Johari-Goldstein mode.
It is related to brittle-ductile transition.
String like correlation motions are observed in Johari-Goldstein relaxation.

Johari-Goldstein relaxation in Metallic glass

$Zr_{47}Cu_{47}Al_7$

Embedded Atom Method potential

Y.Q. Cheng, et al.,
Phys. Rev. Lett. 102, 245501 (2009).

Density

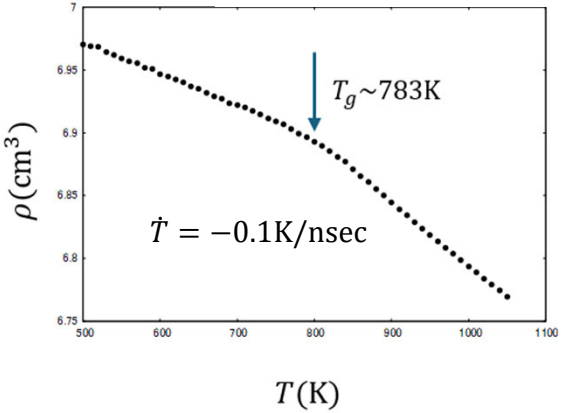

Scattering function

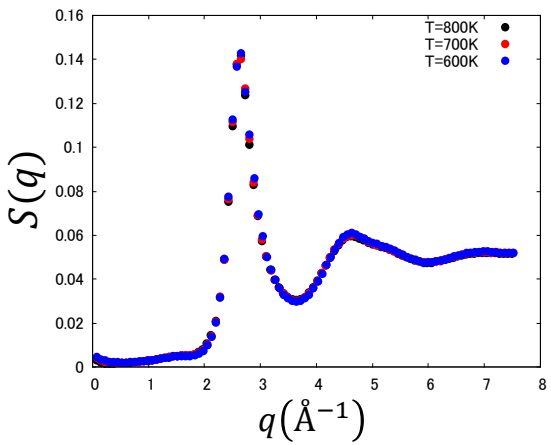

Dynamic mechanical analysis

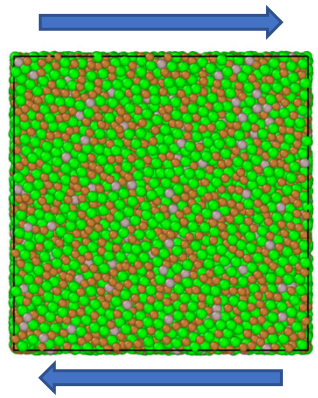

$\gamma(t) = \gamma_0 \sin(2\pi t/\tau)$

Loss modulus

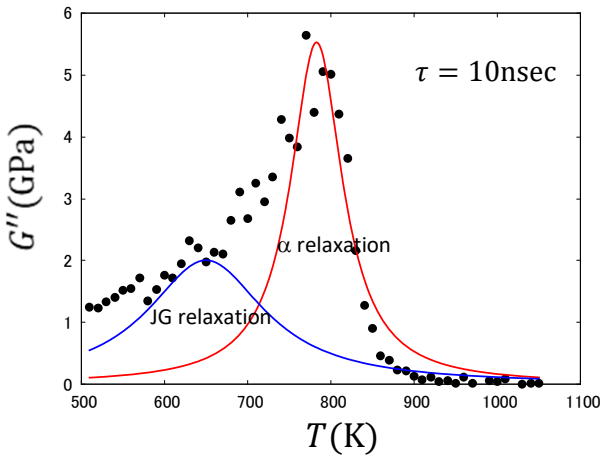

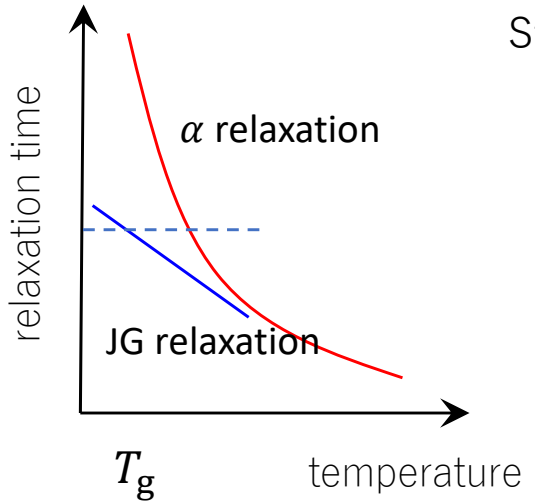

Stress relaxation after $\gamma = 0.05$ deformation

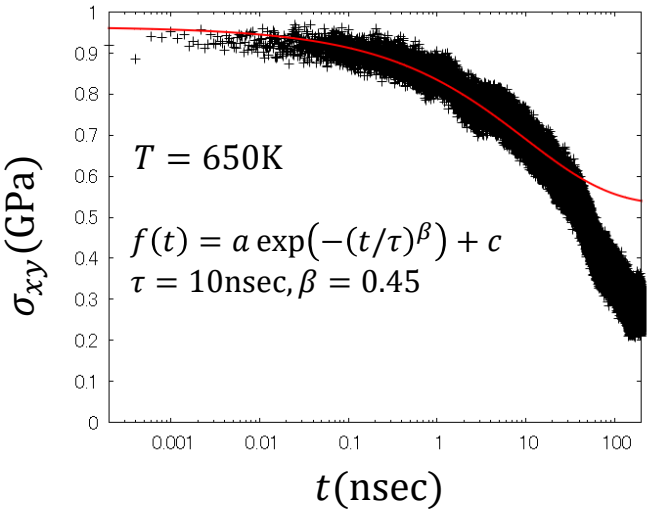

Johari-Goldstein relaxation in metallic glass

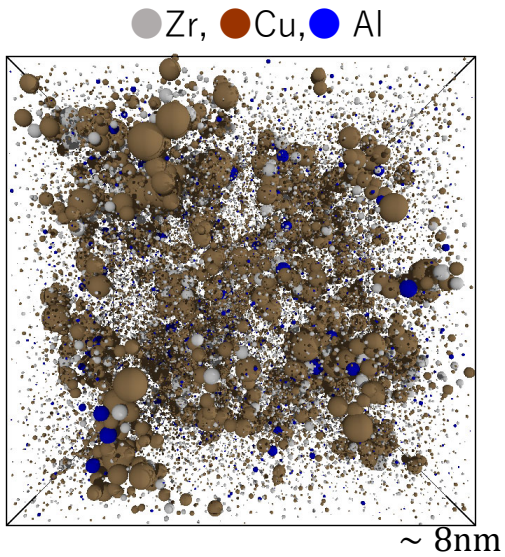

Particle size:
displacement in 10nsec

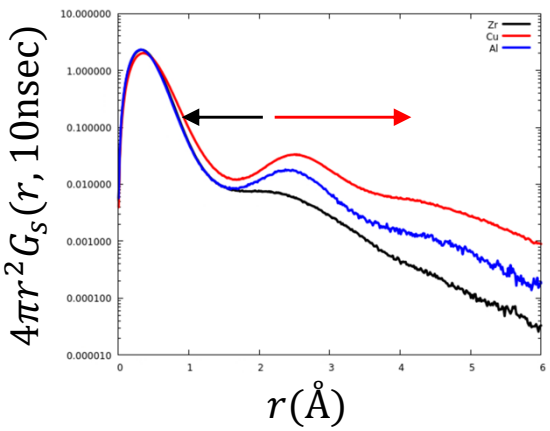

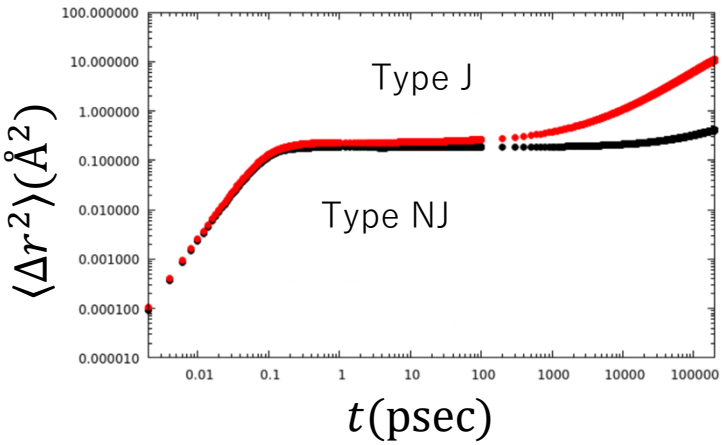

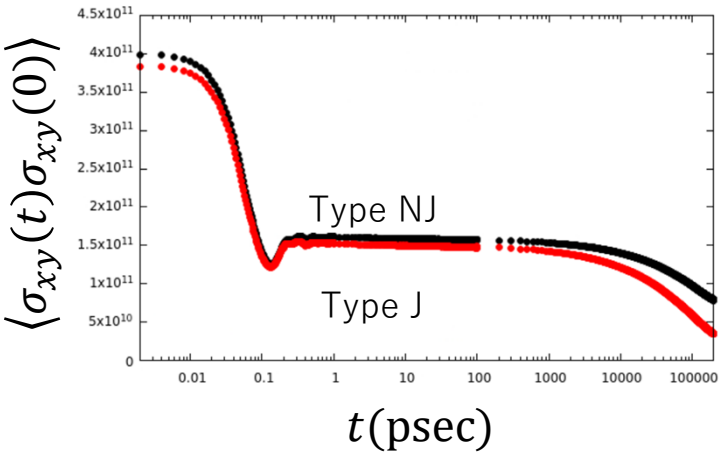

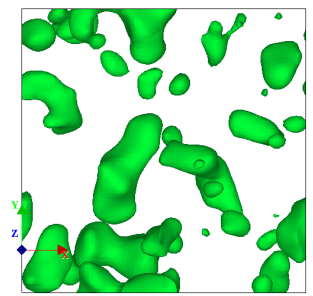

90% of structure relaxation

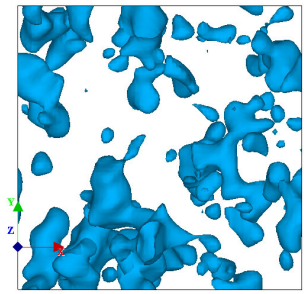

80% of stress relaxation

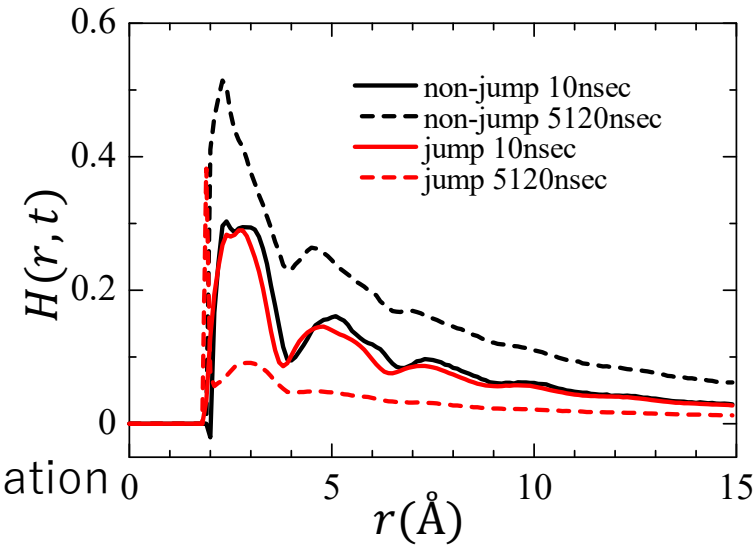

MSD and stress auto-correlation

The behaviors observed in metallic glasses are essentially the same as those in an ionic glass. Universal picture of Johari-Goldstein relaxation mode?

Summary

We carried out molecular dynamics simulation of ionic glass CKN and metallic glass ZrCuAl.
(Rotational and internal motions can be ignored.)

We reproduced the experimental results for CKN quantitively.

We found that the unexpected collective motion of non-jumping particles in the JG time scale in both systems.

The thermally activated jumps cause the small motions and the stress relaxation around them.

These similarity suggests the universal picture of our finding on the JG-relaxation mode.